J|A|C|S ARTICLES

Published on Web 11/30/2009

Effect of Peptide Fragment Size on the Propensity of Cyclization in Collision-Induced Dissociation: Oligoglycine b_2-b_8

Xian Chen,[†] Long Yu,[†] Jeffrey D. Steill,[‡] Jos Oomens,[‡,§] and Nick C. Polfer*[,†]

Department of Chemistry, University of Florida, Gainesville, Florida 32611, FOM Institute for Plasma Physics 'Rijnhuizen', Edisonbaan 14, 3439 MN Nieuwegein, The Netherlands, and University of Amsterdam, Nieuwe Achtergracht 166, 1018 WV Amsterdam, The Netherlands

Received April 17, 2009; E-mail: polfer@chem.ufl.edu

Abstract: The chemistry of peptide fragmentation by collision-induced dissociation (CID) is currently being reviewed, as a result of observations that the amino acid sequence of peptide fragments can change upon activation. This rearrangement mechanism is thought to be due to a head-to-tail cyclization reaction, where the N-terminal and C-terminal part of the fragment are fused into a *macrocycle* (= cyclic peptide) structure, thus "losing" the memory of the original sequence. We present a comprehensive study for a series of **b** fragment ions, from $\mathbf{b_2}$ to $\mathbf{b_8}$, based on the simplest amino acid residue glycine, to investigate the effect of peptide chain length on the appearance of *macrocycle* fragment structures. The CID product ions are structurally characterized with a range of gas-phase techniques, including isotope labeling, infrared photodissociation spectroscopy, gas-phase hydrogen/deuterium exchange (using CH_3OD), and computational structure approaches. The combined insights from these results yield compelling evidence that smaller $\mathbf{b}_n$ fragments ($n = 2, 3$) exclusively adopt *oxazolone*-type structures, whereas a mixture of *oxazolone* and *macrocycle* **b** fragment structures are formed for midsized $\mathbf{b}_n$ fragments, where $n = 4-7$. As each of these chemical structures exchanges at different rates, it is possible to approximate the relative abundances using kinetic fits to the H/D exchange data. Under the conditions used here, the "slow"-exchanging *macrocycle* structure represents ~30% of the **b** ion population for $\mathbf{b_6}-\mathbf{b_7}$, while the "fast"-exchanging *oxazolone* structure represents the remainder (70%). Intriguingly, for $\mathbf{b_8}$ only the *macrocycle* structure is identified, which is also consistent with the "slow" kinetic rate in the HDX results. In a control experiment, a protonated cyclic peptide with 6 amino acid residues, cyclo(Gln-Trp-Phe-Gly-Leu-Met), is confirmed not to adopt an *oxazolone* structure, even upon collisional activation. These results demonstrate that in some cases larger *macrocycle* structures are surprisingly stable. While more studies are required to establish the general propensity for cyclization in **b** fragments, the implications from this study are troubling in terms of faulty sequence identification.

1. Introduction

Knowledge of the primary structure (i.e., amino acid sequence) of a peptide/protein is essential in unambiguous identification. Historically, Edman degradation was the method of choice for determining the sequences of proteins. Since the 1990s, tandem mass spectrometry has taken over this role, mainly because of its increased sensitivity and ability to cope with complex mixtures.[1,2] The most popular approach involves colliding proton-attached peptides with a background gas to cause collision-induced dissociation (CID). This results in efficient cleavage of the amide bond on the peptide backbone, leading to N-terminal "**b**" and C-terminal "**y**" product ions, according to the nomenclature of Roepstorff.[3,4] Mechanistically, it is commonly accepted that **y** fragments adopt a linear peptide structure with an N-terminal amino group. Conversely, numerous chemical structures have been proposed for **b** fragments over the years.[5,6] The *acylium* structure[4] has been rejected on the grounds that it would spontaneously lose a CO moiety from its C-terminal side.[7−9] Stabilizing the C-terminal carbonyl group in a **b** fragment requires a nucleophilic attack at this site. Depending on the primary structure of the peptide, a multitude of nucleophilic groups are in principle available to take part in such a reaction. The five-membered ring *oxazolone* structure, originally proposed by Harrison,[7] involves a nucleophilic attack from the adjacent carbonyl oxygen on the N-terminal side. The *diketopiperazine* $\mathbf{b_2}$ structure, originally proposed by Wesdemiotis,[10,11] results from nucleophilic attack by the N-terminal amine

[†] University of Florida.
[‡] FOM Institute for Plasma Physics 'Rijnhuizen'.
[§] University of Amsterdam.

(1) Biemann, K.; Martin, S. A. *Mass Spectrom. Rev.* **1987**, *6*, 1–75.
(2) Chait, B. T.; Wang, R.; Beavis, R. C.; Kent, S. B. *Science* **1993**, *262*, 89–92.
(3) Roepstorff, P.; Fohlmann, J. *J. Biomed. Mass Spectrom.* **1984**, *11*, 601.
(4) Biemann, K. *Biomed. Environ. Mass Spectrom.* **1988**, *16*, 99–111.
(5) Harrison, A. G. *Mass Spectrom. Rev.* **2009**, *28*, 640–654.
(6) The chemical structure notation will be highlighted in cursive text throughout the manuscript.
(7) Yalcin, T.; Khouw, C.; Csizmadia, I. G.; Peterson, M. R.; Harrison, A. G. *J. Am. Soc. Mass Spectrom.* **1995**, *6*, 1165–1174.
(8) Yalcin, T.; Csizmadia, I. G.; Peterson, M. B.; Harrison, A. G. *J. Am. Soc. Mass Spectrom.* **1996**, *7*, 233–242.
(9) Paizs, B.; Lendvay, G.; Vekey, K.; Suhai, S. *Rapid Commun. Mass Spectrom.* **1999**, *13*, 525–533.
(10) Cordero, M.; Houser, J.; Wesdemiotis, C. *Anal. Chem.* **1993**, *65*, 1594–1601.

 10.1021/ja9030837

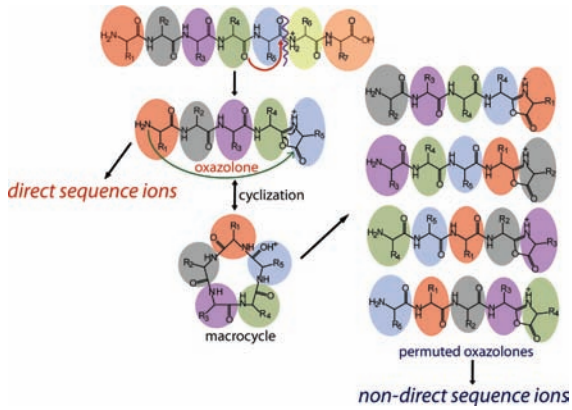

Figure 1. Scheme showing sequence "scrambling" mechanism in collision-induced dissociation of peptides, based on the mechanism proposed by Paizs:[17] dissociation of the amide bond between the 5th and 6th amino acid residues gives rise to an *oxazolone* $\mathbf{b_5}$ fragment, which can then isomerize to a *macrocycle* structure. When this *macrocycle* opens up, it can result in either *oxazolone* structures with the original sequence or permuted sequences. Sequential fragmentation of the original oxazolone leads to direct sequence ions, whereas fragmentation of the permuted *oxazolones* leads to **non**direct sequence ions in the tandem mass spectra.

nitrogen. Finally, side-chain nucleophiles, such as lysine amine, arginine guanine, and histidine imidazole groups have been proposed to act as nucleophiles by O'Hair, Wysocki, and others.[12−16] In terms of determining the amino acid sequence of a peptide, particularly the second reaction presents a problem,[17] especially if this occurs for larger $\mathbf{b}_n$ fragments, where $n > 2$. In such a *macrocycle*, the memory of the original primary structure is lost, if reopening of the ring takes place at a different site than where it was initially put together.

One of the first observations of gas-phase rearrangement reactions in CID was observed by Boyd and co-workers.[18,19] Vachet and Glish described such rearrangement processes for an **a**-type fragment in Leu-enkephalin.[20] Harrison and Paizs have demonstrated this sequence "scrambling" phenomenon for **b** fragments in the case of the enkephalin pentapeptide Tyr-Ala-Gly-Phe-Leu-NH_2, where they observed *nondirect* sequence product ions (i.e., product ions that do not reflect the original sequence of the peptide).[17] These results were comparable to the CID of the cyclic counterpart, cyclo(Tyr-Ala-Gly-Phe-Leu), of this peptide. Paizs proposed a mechanism, by which an *oxazolone* structure is initially formed, which can then isomerize to a *macrocycle* structure via a low-energy pathway. This mechanism is illustrated in Figure 1 for the example of a $\mathbf{b_5}$ fragment. Reopening of the *macrocycle* structure leads to *oxazolone* structures with permuted sequences, which give rise to *nondirect* sequence ions. Similar trends in sequence scrambling fragmentation pathways of protonated peptides have been put forward by Bleiholder et al. for a number of C-terminal amidated pentapeptides.[21]

Direct evidence for *macrocycle* structures has come from infrared photodissociation spectroscopy[22,23] and ion mobility.[24,25] Polfer et al. have shown that the IR spectrum of the $\mathbf{b_4}$ fragment of the enkephalin peptide Tyr-Gly-Gly-Phe-Leu displays a prominent band at 1440 cm^{-1}, which was assigned to the $CO-H^+$ bending mode of the *cyclic* structure.[26] Recently, Maitre and co-workers presented compelling evidence for exclusive *macrocycle* structure formation for $\mathbf{b_5}$ from G_5R,[27] showing the complete absence of *oxazolone*-type structures. Garcia and Gaskell were able to separate two structures for the $\mathbf{b_5}$ fragment of the enkephalin Tyr-Ala-Gly-Phe-Leu-NH_2 peptide using ion mobility mass spectrometry.[28] The most compact $\mathbf{b_5}$ fragment structure had a mobility equivalent to that of the cyclic peptide cyclo(Tyr-Ala-Gly-Phe-Leu). They have also applied this technique to larger **b** fragments (up to $\mathbf{b_8}$).[29] Although the ion mobility distributions were too broad to resolve the structures present, they did observe differences in the CID patterns when selecting the leading or trailing edges of the distribution. Polfer et al. could successfully separate and quantify multiple structures of the $\mathbf{a_4}$ fragment from enkephalin Tyr-Gly-Gly-Phe-Leu.[30] They merely observed one distribution for the $\mathbf{b_4}$ fragment of this peptide, even though the width of the mobility distribution was wider that than for the reference compound, N-acetylated Tyr-Gly-Gly-Phe-Leu, which cannot give rise to a cyclic $\mathbf{b_4}$ structure. These preliminary studies seem to indicate that ion mobility is not always capable of separating *oxazolone* and *macrocycle* **b** fragment structures, and hence additional approaches may be required.

Other gas-phase techniques that have been used to characterize CID product structures include gas-phase hydrogen−deuterium exchange (HDX)[31,32] and blackbody infrared radiative dissociation (BIRD).[33,34] O'Hair and co-workers employed HDX to investigate a series of **b** fragments made from oligoglycines, where they considered several water loss reaction channels.[35] Wysocki and Somogyi have employed HDX to determine that **b** ions often exhibit bimodal distributions, which can be rationalized by the presence of two different chemical struct-

(11) Polce, M. J.; Ren, D.; Wesdemiotis, C. *J. Mass Spectrom.* **2000**, *35*, 1391–1398.
(12) Wysocki, V. H.; Tsaprailis, G.; Smith, L. L.; Breci, L. A. *J. Mass Spectrom.* **2000**, *35*, 1399–1406.
(13) Farrugia, J.; O'Hair, R. A. J.; Reid, G. *Int. J. Mass Spectrom.* **2001**, *210/211*, 71–87.
(14) Huang, Y.; Wysocki, V. H.; Tabb, D. L.; Yates, J. R. *Int. J. Mass Spectrom.* **2002**, *219*, 233–244.
(15) Kish, M. M.; Wesdemiotis, C. *Int. J. Mass Spectrom.* **2003**, *227*, 191–201.
(16) Farrugia, J.; O'Hair, R. A. J. *Int. J. Mass Spectrom.* **2003**, *222*, 229–242.
(17) Harrison, A. G.; Young, A. B.; Bleiholder, B.; Suhai, S.; Paizs, B. *J. Am. Chem. Soc.* **2006**, *128*, 10364–10365.
(18) Tang, X.; Thibault, P.; Boyd, R. K. *Anal. Chem.* **1993**, *65*, 2824–2834.
(19) Tang, X.; Boyd, R. K. *Rapid Commun. Mass Spectrom.* **1994**, *8*, 678–686.
(20) Vachet, R. W.; Bishop, B. M.; Erickson, B. W.; Glish, G. L. *J. Am. Chem. Soc.* **1997**, *119*, 5481–5488.
(21) Bleiholder, C.; Osburn, S.; Williams, T.; Suhai, S.; van Stipdonk, M. J.; Harrison, A. G.; Paizs, B. *J. Am. Chem. Soc.* **2008**, *130*, 17774–17789.
(22) Eyler, J. R. *Mass Spectrom. Rev.* **2009**, *28*, 448–467.
(23) Polfer, N. C.; Oomens, J. *Mass Spectrom. Rev.* **2009**, *28*, 468–494.
(24) Clemmer, D. E.; Jarrold, M. F. *J. Mass Spectrom.* **1997**, *32*, 577–592.
(25) Wyttenbach, T.; Bowers, M. T. *Top. Curr. Chem.* **2003**, *225*, 207–232.
(26) Polfer, N. C.; Oomens, J.; Suhai, S.; Paizs, B. *J. Am. Chem. Soc.* **2007**, *129*, 5887–5897.
(27) Erlekam, U.; Bythell, B.; Scuderi, D.; Van Stipdonk, M. J.; Paizs, B.; Maitre, P. *J. Am. Chem. Soc.* **2009**, *131*, 11503–11508.
(28) Garcia, I.; Giles, K.; Bateman, R. H.; Gaskell, S. J. *J. Am. Soc. Mass Spectrom.* **2008**, *19*, 609–613.
(29) Garcia, I.; Giles, K.; Bateman, R. H.; Gaskell, S. J. *J. Am. Soc. Mass Spectrom.* **2008**, *19*, 1781–1787.
(30) Polfer, N. C.; Bohrer, B. C.; Plasencia, M. D.; Paizs, B.; Clemmer, D. E. *J. Phys. Chem. A* **2008**, *112*, 1286–1293.
(31) Campbell, S.; Rodgers, M. T.; Marzluff, E. M.; Beauchamp, J. L. *J. Am. Chem. Soc.* **1995**, *117*, 12840–12854.
(32) Green, M. K.; Lebrilla, C. B. *Mass Spectrom. Rev.* **1997**, *16*, 53–71.
(33) Dunbar, R. C.; McMahon, T. B. *Science* **1998**, *29*, 194–197.
(34) Schnier, P. D.; Price, W. D.; Strittmatter, E. F.; Williams, E. R. *J. Am. Soc. Mass Spectrom.* **1997**, *8*, 771–780.

ures.[36,37] Paizs and Somogyi have used H/D exchange and DFT calculations for trypic digest peptide $\mathbf{b_2}$ fragments to show that exclusively *oxazolone* structures are formed.[38] Nonetheless, the interpretation of HDX data is complicated by an inadequate understanding of the HDX mechanism, thus making direct structural assignment difficult. Finally, stable isotope labeling techniques have been used by many groups for the mechanistic elucidation of gas-phase reactions and fragmentations over the years.[29,39−43]

In this paper, we combine isotope labeling, infrared spectroscopy, gas-phase HDX, and computational approaches to structurally characterize a series of CID **b** product ions from $\mathbf{b_2}$ to $\mathbf{b_8}$ generated from oligoglycine peptides. In these systems, no side-chain nucleophiles are present, and hence the competition between *oxazolone* and *macrocycle* formation can be studied as a function of size of the fragment generated. The different insights from these studies present strong evidence that the occurrence of *macrocycle* **b** structures is size-dependent.

2. Experimental Section and Calculations

2.1. Mass Spectrometry and Hydrogen/Deuterium Exchange. The hydrogen/deuterium exchange (HDX) experiments were carried out at the University of Florida using a commercially available Fourier transform ion cyclotron resonance (FT-ICR) mass spectrometer (4.7 T actively shielded APEX II, Bruker Daltonics, Billerica, MA). The peptides triglycine and pentaglycine (Sigma Aldrich, St. Louis, MO) were employed without further purification. Octaglycine was prepared by solid-phase synthesis and was isotopically labeled by incorporating a ^{13}C-Gly as the N-terminal residue (ICBR, University of Florida). The peptide was purified by high-performance liquid chromatography (HPLC). All peptides were ionized by electrospray ionization (ESI) in 49:49:2 water/methanol/acetic acid solutions at 20 μM. The protonated peptide precursor ions were activated by "nozzle-skimmer" dissociation in the ESI source region by adjusting the voltage drop between the metal-plated glass capillary and the first skimmer. The CID product ions were then accumulated in the hexapole (3−4 s), prior to transfer to the ICR cell. The exception to this was the $\mathbf{b_2}$ (*m*/*z* 115) fragment, which was generated in the ICR cell by sustained off-resonance irradiation collision-induced dissociation (SORI-CID) from protonated triglycine by pulsing in Xe gas, as low-*m*/*z* (<130) ions could not be transferred from the hexapole to the ICR cell successfully.[44] The fragment $\mathbf{b_4}$ was made from pentaglycine by nozzle-skimmer dissociation. A series from $\mathbf{b_5}$−$\mathbf{b_8}$ was prepared from octaglycine, as well as a low abundance peak of $\mathbf{b_3}$.

The most abundant isotope peak of the $\mathbf{b}_n$ product ion of interest was mass isolated and subjected to gas-phase hydrogen−deuterium exchange (HDX) with CH_3OD, which was leaked into the vacuum chamber at a constant pressure of $\sim 10^{-8}$ Torr.[45] Mass spectra with different exchange times were recorded, and the abundances for the undeuterated (d_0), singly deuterated (d_1), etc. peaks in the resulting distributions were determined. The data are represented here by plotting the natural logarithm of the ratio of d_0 divided by the sum of all ions, $\ln[d_0/\Sigma d_n]$, as a function of the HDX time, as previously reported.[46,47] The depletion of d_0 is also represented as a percentage (i.e., $[d_0/\Sigma d_n] \times 100$), which is plotted on a natural logarithm scale.

2.2. Mass Spectrometry and Infrared Photodissociation Spectroscopy. The infrared photodissociation experiments were conducted at the FOM institute for Plasma Physics "Rijnhuizen" using the free electron laser FELIX[48] coupled to a laboratory-built FT-ICR mass spectrometer, described in detail in previous publications.[49,50] The $\mathbf{b_2}$, $\mathbf{b_5}$, and $\mathbf{b_8}$ CID products were generated by "nozzle-skimmer" dissociation, in a similar scheme as described above, using protonated triglycine, pentaglycine, and octaglycine, respectively. The fragment ion was accumulated in the hexapole, prior to transfer to the ICR cell. As a control experiment for $\mathbf{b_2}$, proton-attached cyclo(Gly-Gly) (Bachem, Torrance, CA) was produced by ESI in a separate experiment to measure its IR spectrum. As a control experiment for larger cyclic peptides, the commercially available peptide cyclo-(Gln-Trp-Phe-Gly-Leu-Met) (Bachem, Torrance, CA) was generated as a protonated ion. Following mass isolation, the ion of interest was irradiated with the tunable output from the free electron laser. FELIX produces macropulses (5 μs) that consist of a train of micropulses at a GHz repetition rate. The pulse energy per macropulse is dependent on wavelength, reaching maximum values of ~60 mJ at 12 μm. Typically, 20−30 macropulses were employed to induce efficient photodissociation.

Infrared multiple-photon dissociation (IR-MPD)[51] spectroscopy works on the premise that when the laser frequency is in resonance with a fundamental vibration in the molecule, many photons (tens to hundreds) are absorbed, leading to photodissociation. This manifests itself in the mass spectrum by a depletion of the precursor ion and appearance of photofragments. In the case of $\mathbf{b_2}$-G3 (*m*/*z* 115), generated from triglycine, an abundant photofragment was observed at *m*/*z* 87, which corresponds to a CO loss (i.e., appearance of $\mathbf{a_2}$). Protonated cyclo(Gly-Gly) (*m*/*z* 115) was also found to photodissociate to *m*/*z* 87 ($\mathbf{a_2}$), as well as *m*/*z* 59 ($\mathbf{a_2}$-H_2O). The corresponding photodissociation channels for $\mathbf{b_5}$-G5 (*m*/*z* 286), from pentaglycine were *m*/*z* 125 (unassigned) and 154 ($\mathbf{b_3}$-H_2O). The IR photodissociation spectrum was obtained by plotting the IR-MPD yield as a function of the wavelength, using the following relation: yield $= -\ln[1 - (\Sigma\text{photofragments}/\Sigma\text{all\_ions})]$. Given the many CID product ions generated from octaglycine, the photodissociation products for $\mathbf{b_5}$-G8 and $\mathbf{b_8}$-G8 were not detectable, and hence the IR-MPD depletion spectra are shown here. The funda-

(35) Reid, G. E.; Simpson, R. J.; O'Hair, R. A. J. *Int. J. Mass Spectrom.* **1999**, *191*, 209–230.
(36) Herrmann, K. A.; Kuppannan, K.; Wysocki, V. H. *Int. J. Mass Spectrom.* **2006**, *249/250*, 93–105.
(37) Somogyi, A. *J. Am. Soc. Mass Spectrom.* **2008**, *19*, 1771–1775.
(38) Bythell, B.; Somogyi, A.; Paizs, B. *J. Am. Soc. Mass Spectrom.* **2009**, *20*, 618–624.
(39) O'Hair, R. A. J.; Reid, G. E. *Eur. Mass Spectrom.* **1999**, *5*, 325–334.
(40) Harrison, A. G. *Int. J. Mass Spectrom.* **2001**, *210*, 361–370.
(41) Cooper, T.; Talaty, E.; Grove, J.; Van Stipdonk, M. J.; Suhai, S.; Paizs, B. *J. Am. Soc. Mass Spectrom.* **2006**, 1654–1664.
(42) Bythell, B.; Molesworth, S.; Osburn, S.; Cooper, T.; Paizs, B.; Van Stipdonk, M. J. *J. Am. Soc. Mass Spectrom.* **2008**, *19*, 1788–1798.
(43) Molesworth, S.; Osburn, S.; van Stipdonk, M. J. *J. Am. Soc. Mass Spectrom.* **2009**, *20*, 2174–2181.
(44) In this particular instrument, it was not possible to transfer ions of *m*/*z* < 130 from the hexapole to the ICR cell. It is not clear what this defect is due to, but we suspect that a hexapole misalignment or erroneous high voltage pulsing or a combination of both is at fault.
(45) Note that the background pressure reading on this gauge was typically found to be 1×10^{-9} Torr. The pressure gauge was calibrated for nitrogen, and the gauge reading was affected by the magnetic field. The actual reading was higher when the gauge was removed from the magentic field. We hence estimate the actual pressure of methanol to be $\sim 5 \times 10^{-8}$ Torr.
(46) Chen, X.; Powell, D. H.; Polfer, N. C. *Proceedings from the 56th American Society for Mass Spectrometry Conference*; 2008, Denver, CO, MPMM 334.
(47) Chen, X.; Yu, L.; Oomens, J.; Steill, J. D.; Powell, D. H.; Polfer, N. *Proceedings from the 57th ASMS Conference on Mass Spectrometry and Allied Topics*; 2009, Philadelphia, PA, WOApm3:30.
(48) Oepts, D.; van der Meer, A. F. G.; van Amersfoort, P. W. *Infrared Phys. Technol.* **1995**, *36*, 297–308.
(49) Valle, J. J.; Eyler, J. R.; Oomens, J.; Moore, D. T.; van der Meer, A. F. G.; von Helden, G.; Meijer, G.; Hendrickson, C. L.; Marshall, A. G.; Blakney, G. T. *Rev. Sci. Instrum.* **2005**, *76*, 23103.
(50) Polfer, N. C.; Oomens, J.; Moore, D. T.; von Helden, G.; Meijer, G.; Dunbar, R. C. *J. Am. Chem. Soc.* **2006**, *128*, 517–525.
(51) Bagratashvili, V. N. ; Letokov, V. S.; Makarov, A. A.; Ryabov, E. A. *Multiple Photon Infrared Laser Photophysics and Photochemistry*; Harwood Academic Publishers: Chur, Switzerland, 1985.

mental and practical aspects of IR-MPD spectroscopy have recently been the subject of a number of review articles,[52−56] notably in a special issue on photodissociation of ions in *Mass Spectrometry Reviews*.[22,23,57]

In the photodissociation experiments presented here, the wavelength was scanned from 1200−2000 and 2500−3400 cm^{-1}. Note that in the latter experiments mirrors with a dichroic coating were employed in the laser cavity, to specifically allow reflection (and hence lasing) at the third harmonic, but not at the fundamental wavelength.

2.3. Computational. Calculations were carried out at the High-Performance Computing (HPC) Center at the University of Florida. A procedure for generating candidate structures for the $\mathbf{b_2}$ and $\mathbf{b_5}$ glycine-based fragments was developed in-house. The chemical structures (*oxazolone*, *diketopiperazine*, and *macrocycle*) were built and optimized using semiempirical approaches (AM1) in HyperChem (Hypercube Inc., Gainesville, FL), also taking into account their preferred sites of proton attachment. In the case of *oxazolones*, proton attachment at both the N-terminus and *oxazolone* ring nitrogen was considered. Proton attachment at a backbone carbonyl is also possible in principle; however, it has been shown that such a structure is much less favored energetically (>30 kJ mol^{-1}).[26] For the *macrocycle* structure, on the other hand, backbone carbonyl oxygens represent the preferred sites of proton attachment. As all of the **b** fragments considered here are exclusively made up of glycine residues, all carbonyl sites are in fact equivalent. The chemical notation previously employed by Polfer et al. will be used here.[26]

One additional chemical family of **b** structures was considered for $\mathbf{b_5}$-G5, which arises for water loss reaction pathways.[35,58] A number of dehydrated structures were in fact proposed by O'Hair and co-workers,[35] having nonterminal five- and six-membered rings. Here, we have considered five-membered ring structures, which are referred to as $[M + H - H_2O]^+$. For these structures, proton attachment at the N-terminus, ring-N and C=N were considered. They were also initially built in Hyperchem, as described above.

All input structures were optimized using density functional theory (DFT) (B3LYP/6-31 g*) methods in Gaussian03,[59] and atomic point charges were derived using electrostatic potential[60] fitting with *ab initio* methods (HF/6-31 g*) in the same program.

The geometry and ESP-derived charges were imported into the AMBER[61] suite of programs, where a restrained electrostatic potential (RESP)[62] fitting was performed. Each chemical structure was parametrized separately in AMBER, followed by a conformational search using simulated annealing cycles. Two separate runs with starting temperatures at 300 and 500 K were carried out, resulting in 100 candidate structures per dynamics simulation.

All output structures from AMBER were then optimized at the DFT level, initially using B3LYP/3-21 in Gaussian03. Further optimization was performed both at the B3LYP/6-31G(d) and finally at the B3LYP/6-31G+(d,p) levels. The electronic energy for each conformer at the B3LYP/6-31G+(d,p) level was corrected for the zero-point energy (ZPE) at the same level to yield the final ZPE-corrected energies. All energies are presented here relative to the lowest-energy conformers found for the $\mathbf{b_2}$ and $\mathbf{b_5}$ fragments respectively. The frequency spectra of the lowest-energy structures at the B3LYP/6-31G+(d,p) level are scaled by 0.98 in the 1200−2000 cm^{-1} range and by 0.965 in the 2400−3500 cm^{-1} range. Both of these scaling factors have successfully been employed for these types of molecules with this level of theory[26,63] and are compatible with values used in the literature.[64−67] Stick spectra were convoluted using a 25 cm^{-1} full width at half-maximum (fwhm) Gaussian profile to allow easier comparison with the recorded IR photodissociation spectra.

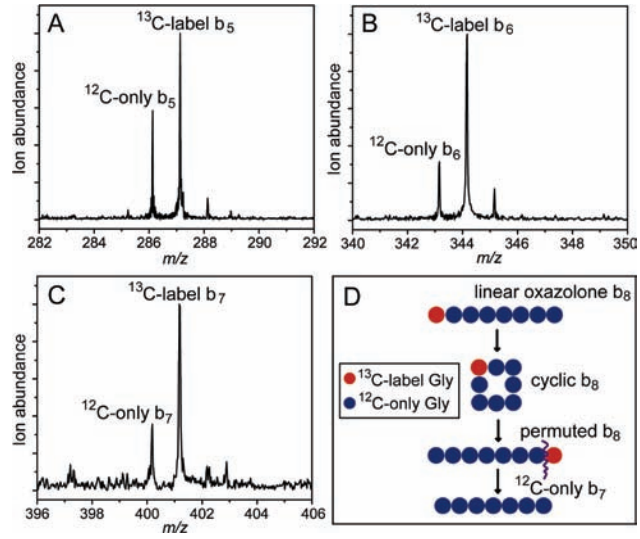

Figure 2. Inserts from the nozzle-skimmer CID spectrum of octaglycine labeled with a ^{13}C-Gly as the N-terminal glycine residue, showing the **b** isotope distributions for (A) $\mathbf{b_5}$, (B) $\mathbf{b_6}$, and (C) $\mathbf{b_7}$. The **^{13}C-label b$_n$** peaks denote **b** ions that incorporate the ^{13}C-Gly label, whereas **^{12}C-only b$_n$** peaks are entirely composed of ^{12}C-Gly residues. (D) The cartoon mechanism rationalizes the appearance of the **^{12}C-only b$_7$** peak.

3. Results and Discussion

3.1. Scrambling in Isotope-Tagged Peptide. In order to test for scrambling in oligoglycine peptides, the octaglycine peptide (made by solid-phase synthesis) was isotopically labeled at the N-terminal position with a ^{13}C glycine residue. CID of the protonated precursor ion (*m/z* 476) resulted not only in $\mathbf{b_n}$ fragments that have this residue incorporated but also in masses where ^{13}C-Gly is apparently eliminated from the molecule. For instance, in the case of $\mathbf{b_7}$, the peak denoted as **^{13}C-label b$_7$** is consistent with the incorporation of the ^{13}C-Gly label, whereas the **^{12}C-only b$_7$** corresponds to the mass exclusively made up of ^{12}C-Gly residues. The loss of N-terminal ^{13}C-Gly from $\mathbf{b_7}$ can be rationalized by a rearrangement process, where $\mathbf{b_8}$ cyclizes and then reopens, resulting in an *oxazolone* with ^{13}C-Gly on the C-terminal side of the molecule (see Figure 2D). Upon amide bond cleavage between the seventh and eighth

(52) Dopfer, O. *Z. Phys. Chem.* **2005**, *219*, 125–168.
(53) Oomens, J.; Sartakov, B. G.; Meijer, G.; von Helden, G. *Int. J. Mass Spectrom.* **2006**, *254*, 1–19.
(54) Polfer, N. C.; Oomens, J. *Phys. Chem. Chem. Phys.* **2007**, *9*, 3804–3817.
(55) Asmis, K. R.; Sauer, J. *Mass Spectrom. Rev.* **2007**, *26*, 542–562.
(56) MacAleese, L.; Maitre, P. *Mass Spectrom. Rev.* **2007**, *26*, 583–605.
(57) Fridgen, T. D. *Mass Spectrom. Rev.* **2009**, *28*, 586–607.
(58) Ballard, K. D.; Gaskell, S. J. *J. Am. Soc. Mass Spectrom.* **1993**, *4*, 477–481.
(59) Frisch, M. J.; et al. *Gaussian 03*, revision C.02; Gaussian, Inc.: Wallingford, CT, 2004.
(60) Ding, Y. B.; Krogh-Jesperson, K. *Computat. Chem.* **1996**, *17*, 338–349.
(61) Cornell, W. D.; Cieplak, P.; Bayly, C. I.; Gould, I. R.; Merz, K., M.; Ferguson, D. M.; Spellmeyer, D. C.; Fox, T.; Caldwell, J. W.; Kollmann, P. A. *J. Am. Chem. Soc.* **1995**, *117*, 5179–5197.
(62) Cieplak, P.; Cornell, W. D.; Bayly, C. I.; Kollmann, P. A. *Computat. Chem.* **1995**, *16*, 1357–1377.
(63) Polfer, N.; Paizs, B.; Snoek, L. C.; Compagnon, I.; Suhai, S.; Meijer, G.; von Helden, G.; Oomens, J. *J. Am. Chem. Soc.* **2005**, *127*, 8571–8579.
(64) Kapota, C.; Lemaire, J.; Maitre, P.; Ohanessian, G. *J. Am. Chem. Soc.* **2004**, *126*, 1836–1842.
(65) Sinha, P.; Boesch, S.; Gu, C.; Wheeler, R.; Wilson, A. *J. Phys. Chem. A* **2004**, *108*, 9213–9217.
(66) Oh, H.; Lin, C.; Hwang, H. Y.; Zhai, H.; Breuker, K.; Zabrouskov, V.; Carpenter, B. K.; McLafferty, F. W. *J. Am. Chem. Soc.* **2005**, *127*, 4076–4083.
(67) Maitre, P.; Lemaire, J.; Scuderi, D. *Phys. Scr.* **2008**, *78*, 058111.

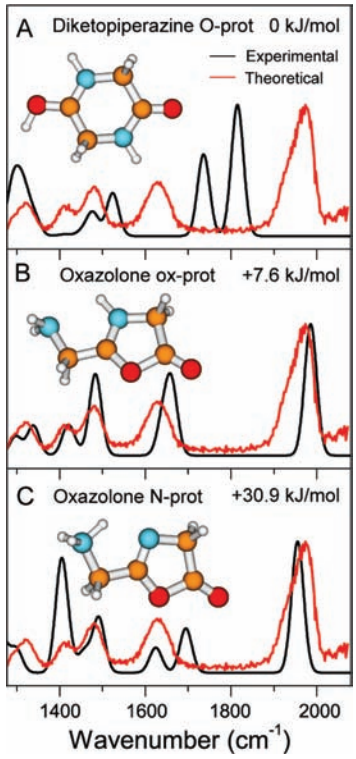

Figure 3. IR-MPD spectrum of the $\mathbf{b_2}$-G3 fragment generated from Gly-Gly-Gly, compared to computed spectra for (A) diketopiperazine structure protonated on a carbonyl O, (B) oxazolone structure protonated on the oxazolone ring N, and (C) oxazolone structure protonated on the N-terminus.

residues, ^{13}C-Gly is then lost as a neutral fragment, yielding **^{12}C-only b$_7$**. The relative abundances of these **^{12}C-only b** ions increases, as one goes down the series from $\mathbf{b_7}$ to $\mathbf{b_5}$. This is not surprising, as the loss of ^{13}C-Gly becomes statistically more likely for smaller fragments. All of these results are consistent with the hypothesis that cyclization in these peptides occurs, followed by sequence scrambling and the appearance of nondirect **b** ions.

3.2. Infrared Spectroscopy Results. A $\mathbf{b_2}$ fragment (*m/z* 115) was generated by subjecting protonated triglycine to CID. For this $\mathbf{b_2}$-G3 fragment, a number of chemical structures have to be considered, including an *oxazolone* structure protonated on the N-terminus (*oxazolone N-prot*), an *oxazolone* structure protonated on the oxazolone ring N (*oxazolone ox-prot*), and a cyclic *diketopiperazine* structure protonated on a carbonyl O (*diketopiperazine O-prot*). Figure 3 presents a comparison of the experimental spectrum recorded in the mid-IR range (1200−2000 cm^{-1}) with the calculated spectra of the lowest-energy conformer for each chemical structure, along with their structures and relative energies. The detailed electronic energies are given in Table S1 in the Supporting Information. Although molecular mechanics modeling was employed here, very few low-energy conformations were in fact found for each chemical structure, and only the best conformer is shown. Based on the prominent band centered at 1960 cm^{-1}, *oxazolone ox-prot* (Figure 3 B) can be identified unambiguously. Conversely, the *oxazolone N-prot* structure (Figure 3 C) gives a poorer match, suggesting that this structure either is not present at all or is at a much reduced abundance relative to *oxazolone ox-prot*. In fact, the predicted energy gap (>23 kJ mol^{-1}) between both of these structures is considerable, supporting the claim that merely *oxazolone ox-prot* is populated at room temperature. Moreover,

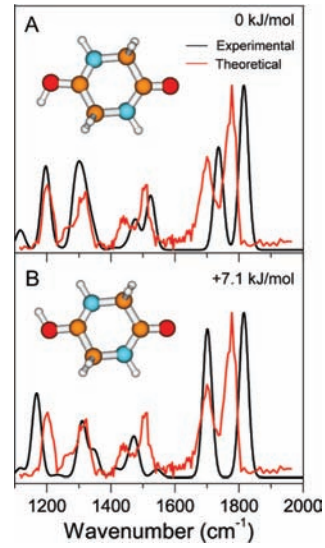

Figure 4. IR-MPD spectrum of protonated cyclo(Gly-Gly), compared to calculated spectra for (A) *diketopiperazine* with proton pointing to CH_2 group and (B) *diketopiperazine* with proton pointing to the amide N−H group.

there is no match between the experimental spectrum and the *diketopiperazine O-prot* structure, despite the fact this structure is marginally lower in energy than *oxazolone ox-prot*. Similar results have also been observed by others for related $\mathbf{b_2}$ fragments, Ala-Ala (from Ala-Ala-Ala) by Oomens and Van Stipdonk and co-workers,[68] Ala-Gly (from Ala-Gly-Gly) by Wysocki and co-workers,[69] and results by Paizs and Maitre and co-workers.[70] The only exception so far to this rule has been the very recent study by Wysocki and co-workers, where the evidence from IR spectroscopy and HDX suggested a mixture of *oxazolone* and *diketopiperazine* structures.[71]

3.2.1. Cyclo(Gly-Gly) Control Experiment. Protonated cyclo(Gly-Gly), cyclo(Gly-Gly)H$^+$, was generated by ESI, and its mid-IR spectrum was recorded with FELIX. As shown in Figure 4, theory predicts the experimental spectrum qualitatively well, even if the scaling factor (0.98) is not optimal for all of the vibrations considered. Subtle differences in the interaction of the proton with the side-chain CH_2 (Figure 4A), as opposed to the amide N−H (Figure 4B), can be distinguished. Collisional activation (in the nozzle-skimmer region of the ESI source) for cyclo(Gly-Gly)H$^+$ gave rise to an identical IR spectrum to Figure 4A (not shown), which confirms that no isomerization takes place between *oxazolone* and *diketopiperazine* structures.

3.2.2. $\mathbf{b_5}$ and $\mathbf{b_8}$ Spectra. The experimental mid-IR-MPD (1200−1940 cm^{-1}) spectra for $\mathbf{b_5}$ (*m/z* 286), generated from proton-attached pentaglycine, $\mathbf{b_5}$-G5, and octaglycine, $\mathbf{b_5}$-G8, as well as $\mathbf{b_8}$ (*m/z* 458), generated from octaglycine, $\mathbf{b_8}$-G8, are overlaid in Figure 5. Clear differences between the spectra can be seen, and these serve as useful guidance in the interpretation of the results. The chemical interpretations of the spectral bands are indicated and are based on comparisons with DFT-calculated spectra for $\mathbf{b_5}$. In contrast to the calculations for $\mathbf{b_2}$, the

(68) Oomens, J.; Young, S.; Molesworth, S.; van Stipdonk, M. J. *J. Am. Soc. Mass Spectrom.* **2009**, *20*, 334–339.
(69) Yoon, S.; Chamot-Rooke, J.; Perkins, B.; Hilderbrand, A. E.; Poutsma, J.; Wysocki, V. H. *J. Am. Chem. Soc.* **2008**, *130*, 17644–17645.
(70) Bythell, B.; Erlekam, U.; Paizs, B.; Maitre, P. *Chem. Phys. Chem.* **2009**, *10*, 883–885.
(71) Perkins, B.; Chamot-Rooke, J.; Yoon, S.; Gucinski, A.; Somogyi, A.; Wysocki, V. H. *J. Am. Chem. Soc.* **2009**, *131*, 17528–17529.

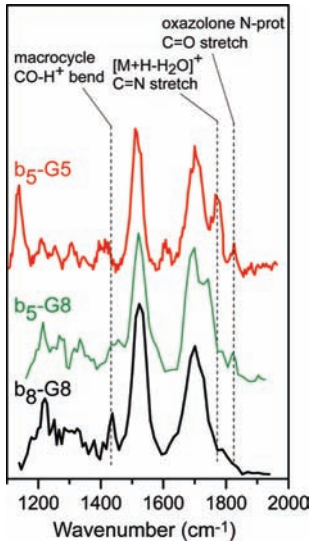

Figure 5. (A) Overlayed mid-IR-MPD spectra of $\mathbf{b_5}$-G5 (from pentaglycine), $\mathbf{b_5}$-G8 (from octaglycine) and $\mathbf{b_8}$-G8 (from octaglycine). The chemically diagnostic modes are indicated.

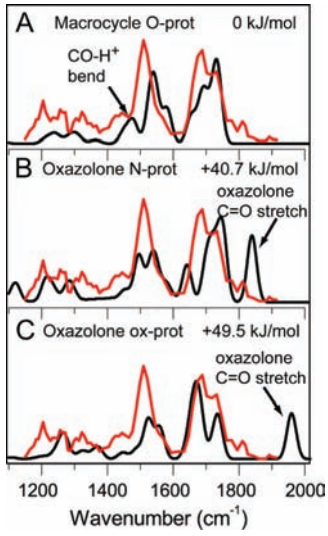

Figure 6. Mid-IR-MPD spectrum of $\mathbf{b_5}$-G8 (generated from octaglycine), compared to the lowest-energy conformers for the various chemical structures: (A) *macrocycle* structure protonated on backbone carbonyl, (B) *oxazolone* structure protonated on N-terminus, and (C) *oxazolone* structure protonated on oxazolone ring N. The relative energies to the lowest conformer are indicated. A more comprehensive summary for the 10 lowest-energy conformers of each chemical structure is shown in the Supporting Information. The chemically diagnostic bands are labeled.

conformational space for $\mathbf{b_5}$ is vastly larger, making molecular mechanics approaches essential in obtaining reliable candidate structures. The two lowest-energy conformers for each chemical structure identified are presented in Figure 6 for comparison with the experimental spectrum of $\mathbf{b_5}$-G8. As a more general summary of our extended study, the energetics, vibrational spectra, and structures for the 10 lowest-energy conformers for each chemical structure are summarized in the Supporting Information (Table S2, Figures S3−8).

3.2.3. Identification of the Macrocycle Structure for $\mathbf{b_8}$. Of the $\mathbf{b_5}$-G5, $\mathbf{b_5}$-G8, and $\mathbf{b_8}$-G8 IR-MPD spectra shown in Figure 5, the spectrum for $\mathbf{b_8}$-G8 is clearly the simplest, lacking some of the spectral features present for $\mathbf{b_5}$-G5 and $\mathbf{b_5}$-G8. For instance, the prominent band at 1775 cm^{-1} for $\mathbf{b_5}$-G5 is not observed for either $\mathbf{b_5}$-G8 or $\mathbf{b_8}$-G8. The weaker feature at 1825 cm^{-1} is observed for both $\mathbf{b_5}$-G5 and $\mathbf{b_5}$-G8, but not for $\mathbf{b_8}$-G8. Recently, Maitre and co-workers showed IR-MPD evidence that $\mathbf{b_5}$ from G_5R exclusively gives rise to a *macrocycle* structure, based on the absence of *oxazolone* bands.[27] The positive identification of the *macrocycle* rests upon unambiguous assignment of modes associated to the proton attachment site on a backbone carbonyl, since this structure is chemically analogous to a peptide backbone and, therefore, lacks other diagnostic chemical moieties. In our comparison of $\mathbf{b_5}$-G5, $\mathbf{b_5}$-G8, and $\mathbf{b_8}$-G8, only $\mathbf{b_8}$-G8 is compatible with the exclusive presence of a *macrocycle* structure, as no *oxazolone* band is observed. Moreover, the presence of the band at ~1430 cm^{-1} indicates the presence of the *macrocycle* structure, as this mode has previously been suggested to be due to the $CO{-}H^+$ (i.e., $(C{=})O{-}H^+$) bending mode of a cyclic peptide structure.[26]

3.2.4. Macrocycle Structure for $\mathbf{b_5}$. The smaller $\mathbf{b_5}$ fragments, $\mathbf{b_5}$-G8 and $\mathbf{b_5}$-G5, also display bands in the 1430 cm^{-1} region, which suggests that both exhibit *macrocycle* structures. This is also confirmed by the computational results, which predict the $CO{-}H^+$ bending mode to occur in this region (see Figure 6). In the case of $\mathbf{b_5}$-G5, the near-IR-MPD range (2500−3300 cm^{-1}) yields information on stretching modes. In Figure S13 (Supporting Information), a broad band is observed between 2500 and 2700 cm^{-1} which is consistent with the predicted $CO{-}H^+$ stretch of the *macrocycle* structure. The exact calculated position of this band is dependent on the conformation. Nonetheless, all of the *macrocycle* structures predict a high-intensity band associated with the $CO{-}H^+$ stretch mode in the 2300−2600 cm^{-1} region. Conversely, none of the *oxazolone* structures have predicted bands in this range (Figures S14 and S15). In the *macrocycle* structure, the proton is partially shared between two carbonyl sites (see Figure S4). This results in a flat anharmonic potential, which is consistent with the broad nature of the 2500−2700 cm^{-1} band. In fact, shared-proton modes are often observed as broad features in IR spectra. For instance, in IR measurements by Johnson and co-workers on proton-bound dimers, the shared proton stretching band was found to be reasonably broad, even for these cold argon-tagged complexes formed in a supersonic expansion.[72,73] For higher temperature proton-bound complexes, the IR-MPD spectral features typically become very broad.[74−77] The broadening of OH stretches as a consequence of strong H-bonding has even been observed in several neutral amino acid and peptide systems.[78,79]

3.2.5. Water Loss $[M + H - H_2O]^+$ Structure for $\mathbf{b_5}$-G5. When comparing the IR-MPD spectra of $\mathbf{b_5}$-G5 and $\mathbf{b_5}$-G8, the

(72) Headrick, J. M.; Diken, E. G.; Walters, R. S.; Hammer, N. I.; Christie, R. A.; Cui, J.; Myshakin, E. M.; Duncan, M. A.; Johnson, M. A.; Jordan, K. D. *Science* **2005**, *308*, 1765–1769.
(73) Roscioli, J. R.; McCunn, L. R.; Johnson, M. A. *Science* **2007**, *316*, 249–254.
(74) Asmis, K. R.; Pivonka, N. L.; Santambrogio, G.; Brummer, M.; Kaposta, C.; Neumark, D. M.; Wöeste, L. *Science* **2003**, *299*, 1375–1377.
(75) Fridgen, T. D.; McMahon, T. B.; MacAleese, L.; Lemaire, J.; Maitre, P. *J. Phys. Chem. A* **2004**, *108*, 9008–9010.
(76) Moore, D. T.; Oomens, J.; van der Meer, A. F. G.; von Helden, G.; Meijer, G.; Valle, J. J.; Marshall, A. G.; Eyler, J. R. *Chem. Phys. Chem.* **2004**, *5*, 740–743.
(77) Fridgen, T. D.; MacAleese, L.; Maitre, P.; McMahon, T. B.; Boissel, P.; Lemaire, J. *Phys. Chem. Chem. Phys.* **2005**, *7*, 2747–2755.
(78) Chin, W.; Compagnon, I.; Dognon, J.-P.; Canuel, C.; Piuzzi, F.; Dimicoli, I.; von Helden, G.; Meijer, G.; Mons, M. *J. Am. Chem. Soc.* **2005**, *127*, 1388–1389.
(79) Inokuchi, Y.; Kobayashi, Y.; Ito, T.; Ebata, T. *J. Phys. Chem. A* **2007**, *11*, 3209–3215.

striking absence of the band at 1775 cm^{-1} is apparent in the case of $\mathbf{b_5}$-G8. As previously reported by O'Hair and co-workers, water loss from protonated peptides can give rise to non-*oxazolone* type fragments.[35] One of the many proposed structures by O'Hair has been investigated here for a structural interpretation of the $\mathbf{b_5}$-G5 spectrum (see Figure S9). A number of probable protonation sites were considered. Of these, proton attachment on the N-terminus (*N-term-prot*) appears to be energetically most favorable (Table S10). Such a structure also predicts a prominent C═N stretching mode at ~1775 cm^{-1}, which appears to confirm the presence of this structure (Figure S11). Moreover, this $[M + H - H_2O]^+$ structure predicts modes that fall in the range of the 2500−2700 cm^{-1} band in the near-IR spectrum, potentially contributing to the broadness of this band (Figure S11). Nonetheless, the number of structural possibilities for $\mathbf{b_5}$-G5 is remarkable, and many more structures would have to be considered. Based on the presence of the 1775 cm^{-1} band, it is clear that $\mathbf{b_5}$-G5 displays a more heterogeneous population of structures than $\mathbf{b_5}$-G8. Moreover, the structural interpretation of $\mathbf{b_5}$-G5 matches many of the diagnostic bands for a number of chemical structures (see Figures S11−S16). Note that a similar IR-MPD study on water loss reaction pathways for $\mathbf{b_4}$ from tetraglycine was undertaken by Van Stipdonk and co-workers, showing similar band positions at ~1775 and ~1825 cm^{-1}.[80] Given the extreme structural heterogeneity of $\mathbf{b_5}$-G5, our subsequent discussions will focus on conventional **b** fragments that are generated along **b**−**y** fragmentation pathways,[81] as opposed to water loss pathways.[35]

3.2.6. Oxazolone Structure for $\mathbf{b_5}$-G8. For the conventional **b** fragment $\mathbf{b_5}$-G8, *oxazolone N-prot* can be identified, based on the diagnostic C═O stretch band associated with the oxazolone ring moiety at ~1825 cm^{-1}, which is in agreement with calculated spectra for this chemical structure (see Figure 6). The corresponding oxazolone C═O stretch of *oxazolone ox-prot* is not observed, though this may be due to our limited scan to 1940 cm^{-1}. Proton attachment on a backbone carbonyl oxygen would also be possible in principle for an *oxazolone* structure; however, such structures are not likely to be substantially populated at room temperature, given their lower proton affinity and, hence, relatively high energetic penalty (>30 kJ mol^{-1}) determined from previous studies.[26]

3.2.7. Trends for $\mathbf{b_2}$, $\mathbf{b_5}$-G8, and $\mathbf{b_8}$-G8. The current results suggest a number of differences between smaller and larger **b** fragments. Namely, $\mathbf{b_2}$ studied here and other $\mathbf{b_2}$ fragments[68−70] exclusively adopt *oxazolone ox-prot* structures. Conversely, **$\mathbf{b_5}$-G8** appears to give a mixture of *oxazolone* and *macrocycle* structures. Finally, the IR-MPD spectrum of **$\mathbf{b_8}$-G8** is consistent with the exclusive presence of *macrocycle* structures.

In summary, IR spectroscopy allows identification of both *oxazolone* and *macrocycle* structures for $\mathbf{b_5}$, based on chemically diagnostic modes. Nonetheless, it is not possible to quantify the relative amounts of both structures, as the IR-MPD intensities cannot reliably be related to ion abundances. Moreover, the photodissociation of *macrocycle* $\mathbf{b_5}$ is expected to require considerably more energy than *oxazolone* $\mathbf{b_5}$,[27] which is likely to result in a lower IR-MPD efficiency of the *macrocycle*. In other words, the IR-MPD experiment in fact discriminates against detection of the *macrocycle* structure.

3.3. Hydrogen−Deuterium Exchange (HDX) Experiments. HDX is employed as a method to quantify the relative amounts of *oxazolone* and *macrocycle* structures formed in CID, as a function of the **b** fragment size. Note that the fragment ions were made by nozzle-skimmer dissociation and that these CID products were accumulated in a hexapole prior to transfer to the ICR cell, as opposed to generating the fragments in the ICR cell by SORI CID (with the exception of $\mathbf{b_2}$-G3, as explained in the Experimental Section and Calculations). This approach presents a number of advantages over in-cell CID. Relatively large and constant number densities of CID product ions can be generated in this manner. Moreover, the pressure of the deuterating agent can be held at a constant pressure, without the need to pulse in a collision gas for SORI CID. Finally, this approach is expected to yield thermalized fragment ions more readily, given the higher-pressure environment in the storage hexapole. As the ion temperature is likely to affect the HDX kinetics, it is important to control the ion temperature in the interest of reproducibility.

The mass spectral distributions for different HDX times for the series $\mathbf{b_2}$−$\mathbf{b_8}$ are shown in Figure S17 in the Supporting Information. These fragments were made from larger precursor ions (tri-, penta-, and octaglycine) to favor **b**−**y** dissociation chemistry,[81] as opposed to water loss pathways.[35] In previous HDX studies bimodal distributions have been observed (for different peptide fragments and systems), which have been explained by the presence of different chemical structures.[36,37] While no obvious bimodal distributions are seen here, a kinetic fitting of the HDX data may reveal the presence of more than one kinetic rate. Note here that for $\mathbf{b_5}$-G5 a bimodal distribution is observed at longer HDX times (see Figure S19) and that this distribution differs significantly from $\mathbf{b_5}$-G8 (Figure S17D). For $\mathbf{b_5}$-G5, a total of five deuterium exchanges are observed, whereas merely three are observed for $\mathbf{b_5}$-G8. This is again consistent with the view that $\mathbf{b_5}$-G5 gives rise to a much more complex population of structures, as opposed to $\mathbf{b_5}$-G8, which is thought to be formed by conventional **b**−**y** dissociation chemistry.

3.3.1. Kinetic Fitting of HDX Data. To determine pseudo-first-order HDX kinetics, the natural logarithm of the relative depletion of the undeuterated peak, $\ln[d_0/\Sigma d_n]$, is plotted as a function of the HDX time. The complete series of HDX measurements from $\mathbf{b_2}$ to $\mathbf{b_8}$ is summarized in Figure 7. Whereas a single kinetic rate ($k = 0.51\ s^{-1}$) is observed in the case of $\mathbf{b_2}$, two distinct kinetic rates are required to fit the data for the larger **b** fragments ($\mathbf{b_4}$-$\mathbf{b_7}$), with the notable exception of $\mathbf{b_8}$. The relative contributions of these "fast"- and "slow"-exchanging populations can be approximated by making a simple assumption: at longer HDX times, the "fast"-exchanging population is fully depleted, and the rate of the "slow"-exchanging population can be determined accurately. A least-squares linear regression fit is employed to determine both the pseudo-first-order rate constant and the intercept. More conveniently, the depletion of d_0 can also be represented as remaining d_0(%) on a natural logarithm scale. It is then found that the intercept of the "slow"-exchanging linear regression fit represents the relative abundance of the "slow"-exchanging structure at time zero. In the case of $\mathbf{b_5}$-G8, the intercept equates to a relative abundance of ~23% for the "slow"-exchanging structure at the beginning of the experiment. By default, the "fast"-exchanging structure accounts for the remainder (~77%). Note that the higher rate at shorter HDX times in Figure 7 corresponds to the combined depletion rates of the "fast"- and "slow"-exchanging structures. Both "fast" and "slow" rates can be

(80) van Stipdonk, M. J.; Bythell, B.; Dain, R.; Oomens, J.; Steill, J. D.; Groenewold, G. S.; Paizs, B. *Proceedings of the 57th ASMS Conference on Mass Spectrometry and Allied Topics*; 2009, Philadelphia, PA, WPMM 666.
(81) Paizs, B.; Suhai, S. *J. Am. Soc. Mass Spectrom.* **2004**, *15*, 103–113.

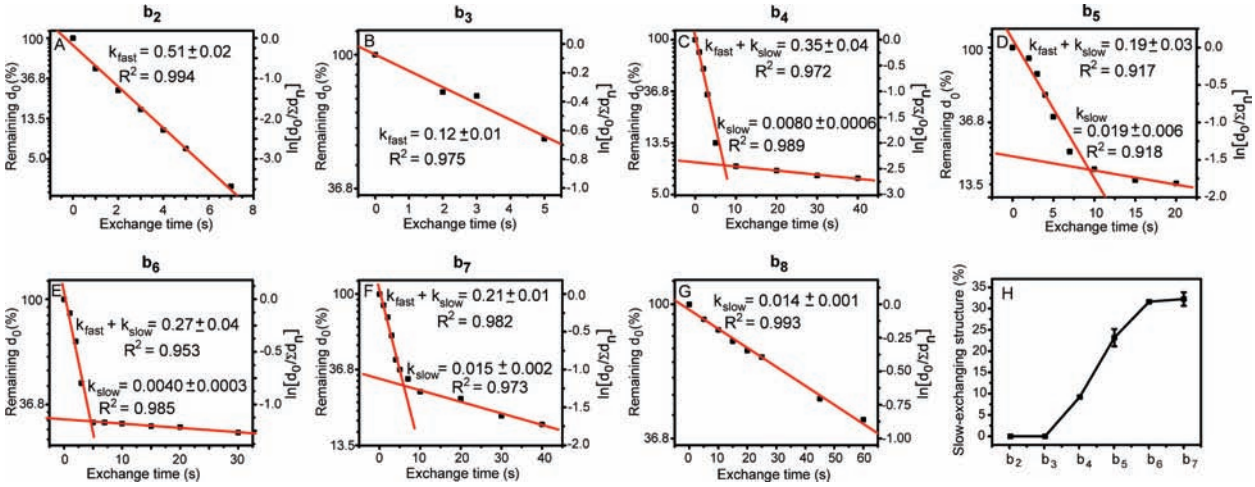

Figure 7. Kinetic fitting of the HDX results for glycine-based **b** fragment ions for (A) $\mathbf{b_2}$ generated from triglycine, (B) $\mathbf{b_3}$ generated from octaglycine, (C) $\mathbf{b_4}$ generated from pentaglycine, (D) $\mathbf{b_5}$ generated from octaglycine, (E) $\mathbf{b_6}$ generated from octaglycine, (F) $\mathbf{b_7}$ generated from octaglycine, and (G) $\mathbf{b_8}$ generated from octaglycine. (H) Relative abundance of "slow"-exchanging structure as a function of $\mathbf{b}_n$ fragment size.

distinguished, as the difference in rate constant is almost an order of magnitude: $k_{slow} = 0.019\ s^{-1}$ vs $k_{fast} = 0.17\ s^{-1}$ ($= 0.19 - k_{slow}$).

3.3.2. Structural Assignment of "Fast"- And "Slow"-Exchanging Structures. The exclusive presence of *oxazolone ox-prot* structures for $\mathbf{b_2}$, as confirmed by the IR-MPD results, correlates well with the presence of one rate of HDX exchange, which happens to be "fast". On the other hand, $\mathbf{b_5}$-G8 is shown to have a mixture of *oxazolone* and *macrocycle* structures, based on the IR-MPD results, and this is confirmed by the presence of two distinct HDX rates, where one is "fast"- and the other one is "slow"-exchanging. Finally for $\mathbf{b_8}$-G8, the IR-MPD results are consistent with the exclusive presence of a *macrocycle* structure, while the HDX results for $\mathbf{b_8}$ exhibit merely one rate of exchange, which happens to be "slow". All of these results are consistent with the view that the "slow"-exchanging ions correspond to the *macrocycle* structure, whereas the "fast"-exchanging structure corresponds to the *oxazolone* structure.

3.3.3. Trends in Relative Abundances of "Fast"- And "Slow"-Exchanging Structures for $\mathbf{b_2}-\mathbf{b_8}$. Over the range from $\mathbf{b_2}$ to $\mathbf{b_8}$ the general classification as "fast" and "slow" rates seems to hold, as both rate constants remain within ranges of $k_{fast} = 0.2-0.5\ s^{-1}$ (with the exception of $\mathbf{b_3}$)[82] and $k_{slow} = 0.004-0.02\ s^{-1}$. The "slow"-exchanging structure is not present for $\mathbf{b_2}$ and $\mathbf{b_3}$[82] but only appears at $\mathbf{b_4}$ or larger fragments. The relative abundances of "slow"-exchanging structures from $\mathbf{b_2}$ to $\mathbf{b_7}$ are summarized in Figure 7H, based on the kinetic fitting procedure, described above. The relative abundance of the "slow"-exchanging structure reaches ~30% for $\mathbf{b_7}$, which indicates that the "fast"-exchanging structure still accounts for the majority of the ion population. Note that the error bars in Figure 7H are determined from the standard deviation of the intercept for the linear regression fit for the "slow"-exchanging structure.

The gradual increase of the relative amount of the *macrocycle* structure from $\mathbf{b_4}$ to $\mathbf{b_7}$ shows that *macrocycle* formation becomes more favorable for larger structures. Nonetheless, the sudden disappearance of the "fast" (= oxazolone) structure for $\mathbf{b_8}$ is rather unexpected. It would be interesting to see what would be observed for larger $\mathbf{b}_n$ fragments. Preliminary experiments to generate larger $\mathbf{b}_n$ product ions ($n > 8$) from deca and dodecaglycine were not successful, instead resulting in dehydrated **b** ions, such as $\mathbf{b_9}$-$\mathbf{H_2O}$ and $\mathbf{b_{10}}$-$\mathbf{H_2O}$ (not shown). Further experiments are required to determine under what conditions such fragment ions can be produced.

3.3.4. Comparison to Erlekam et al.[27] Study on $\mathbf{b_5}$ from $\mathbf{G_5R}$. The identical $\mathbf{b_5}$ fragment considered here, but generated from a different precursor ion (G_5R), was investigated by Maitre and co-workers by IR-MPD spectroscopy and computational studies. In that study, no diagnostic bands for *oxazolone* structures were observed, which was interpreted with the exclusive presence of *macrocycle* structures. Conversely, our IR-MPD results for $\mathbf{b_5}$-G8 are compatible with a mixture of *oxazolone* and *macrocycle* structures (bands at 1825 and 1430 cm^{-1}). Moreover, the HDX results indicate that the *macrocycle* only accounts for ~23% of the ion population, whereas the *oxazolone* structure accounts for the majority (77%).

The differences in both studies may be due to kinetic effects due to different methods of ion activation ("nozzle-skimmer" dissociation vs collisional activation in a Paul trap) and different collisional cooling rates. According to the sequential mechanism by Paizs, an *oxazolone* structure is formed along a **b**−**y** fragmentation pathway prior to isomerization to the *macrocycle* structure and followed by sequential ring opening to *oxazolone* structures.[17] It is conceivable that varying ratios of product ions can be formed in different CID conditions. Detailed kinetic studies on peptide dissociation have been carried out by Laskin et al.,[83,84] which have shown that the extent and time scale of energy deposition have an important effect on product ratios in peptide dissociation.

3.3.5. Model Cyclic Peptide. To make this quantitative HDX technique useful for other peptide systems, the hypothesis that *macrocycle* **b** fragment structures have typically slower HDX kinetics than *oxazolone* structures requires further verification. We have chosen cyclo(Gln-Trp-Phe-Gly-Leu-Met) as an ap-

(82) Note that the ion abundance of $\mathbf{b_3}$ was too low to obtain high-quality HDX data. Hence, the magnitude of the kinetic rate cannot be approximated with a high degree of accuracy. Note also that $\mathbf{b_3}$ could only be produced at all from octaglycine, whereas no $\mathbf{b_3}$ could be generated from either tri-, tetra-, or pentaglycine.

(83) Laskin, J.; Futrell, J. H. *J. Chem. Phys.* **2002**, *116*, 4302–4310.
(84) Laskin, J.; Futrell, J. H. *J. Am. Soc. Mass Spectrom.* **2003**, *14*, 1340–1347.

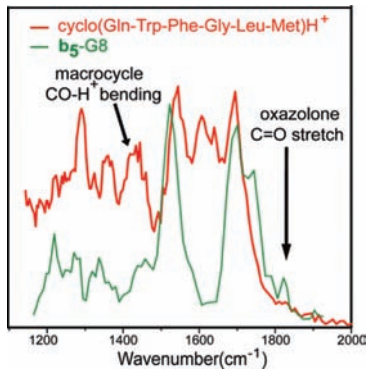

Figure 8. Overlaid IR-MPD spectra of protonated cyclo(Gln-Trp-Phe-Gly-Leu-Met) and $\mathbf{b_5}$-G8. The chemically diagnostic *oxazolone* C=O stretch and *macrocycle* CO−H^+ bending modes are indicated.

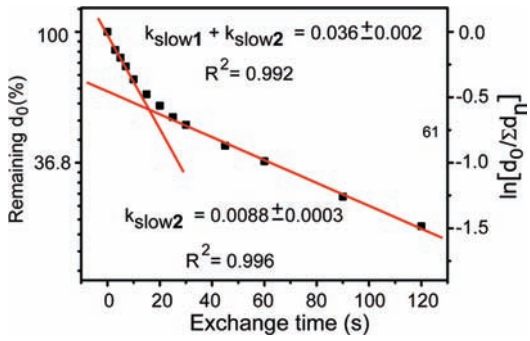

Figure 9. Natural logarithm of relative d_0 depletion, $\ln[d_0/\Sigma d_n]$ (right scale), as a function of time for protonated cyclo(Gln-Trp-Phe-Gly-Leu-Met). The corresponding natural logarithm scale of relative percentage of remaining d_0 is shown to the left.

propriate cyclic peptide model, as this peptide contains no basic amino acids (i.e., arginine, lysine, or histidine), and hence a backbone carbonyl is a likely site of proton attachment.

3.3.6. IR-MPD of Cyclo(Gln-Trp-Phe-Gly-Leu-Met). The IR-MPD spectrum of this protonated cyclo-peptide is contrasted with those of $\mathbf{b_5}$-G5 and $\mathbf{b_5}$-G8 in Figure 8. To promote isomerization from *cyclic* to *oxazolone* structures for this cyclic peptide, harsh source conditions were employed, where some of the protonated cyclo(Gln-Trp-Phe-Gly-Leu-Met) precursor ions were fragmented by nozzle-skimmer CID. Nonetheless, the absence of bands at 1825 cm^{-1} clearly shows that the cyclic peptide does not adopt an *oxazolone* structure, even under these energetic conditions. Conversely, a prominent feature is seen at 1430 cm^{-1}, which is likely assigned to the chemically diagnostic CO−H^+ bending mode.[85] This shows that *macrocycle* peptide structures can be surprisingly stable in the gas phase, thus strengthening the claim that larger cyclic $\mathbf{b}_n$ fragment structures, where $n > 5$, can be formed in CID conditions.

3.3.7. HDX of Cyclo(Gln-Trp-Phe-Gly-Leu-Met). HDX for this cyclic peptide with CH_3OD (under identical conditions as those for the $\mathbf{b_5}$-G8 fragment ions) gave rise to the depletion kinetics for d_0 shown in Figure 9. Two distinct rates of exchange can be resolved. At first sight, it seems that the appearance of two kinetic rates contradicts our hypothesis above, because there is clearly only one chemical isomer present, namely the *macrocyclic* structure. Nonetheless, a closer examination of the magnitudes of the rate constants for cyclo(Gln-Trp-Phe-Gly-Leu-Met)H^+ shows that they are both relatively "slow" compared to the "fast"-exchanging structure for $\mathbf{b_5}$ ($k_1 = 0.027\ s^{-1}$ and $k_2 = 0.009\ s^{-1}$ vs $k_{fast} = 0.17\ s^{-1}$). In fact, both of these rate constants are much more in accordance with the "slow"-exchanging structure for $\mathbf{b_5}$ ($0.02\ s^{-1}$). The absence of an *oxazolone* structure for cyclo(Gln-Trp-Phe-Gly-Leu-Met), as confirmed by IR-MPD spectroscopy, hence correlates well with the absence of a "fast"-exchanging structure in the HDX results. In conclusion, this supports our hypothesis that *macrocycle* fragment structures have HDX exchange rates that are approximately an order of magnitude lower than those of *oxazolone* structures.

At this moment, it is not completely clear what causes the appearance of two distinct "slow" rates for cyclo(Gln-Trp-Phe-Gly-Leu-Met)H^+. It is possible that different protonation sites have to be considered for this peptide, such as the tryptophan indole side chain for instance, or a number of backbone carbonyls. If the structures do not interconvert (i.e., no proton transfer), this may result in multiple exchange kinetics. Alternatively, cyclo(Gln-Trp-Phe-Gly-Leu-Met)H^+ is made up of different structural variants, such as cis−trans isomers for example. In principle, the oligoglycine **b** fragment ions considered here present a much reduced number of conformational possibilities within a given chemical structure, which probably accounts for the presence of a single "slow" rate.

3.3.8. Chemical Basis for Differences in HDX Rates. Given the pronounced chemical differences between *oxazolone* and *macrocycle* **b** fragment structures, and hence differences in their proton affinities (PAs), their HDX rates are expected to differ. Previous studies have shown that *oxazolones* have higher PAs than *macrocycle* structures,[21,26,86] due to the presence of more basic proton attachment sites (i.e., N-terminus and oxazolone ring N, vs backbone carbonyl). In detailed studies by Beauchamp and co-workers[31,87] and Lebrilla and co-workers,[32,88] it has been shown that a smaller difference in proton affinity between the deuterating reagent and the peptide results in faster HDX rates. The above results for *oxazolone* and *macrocycle* $\mathbf{b_5}$-G8 seem to show the opposite effect, as the less basic *macrocycle* structure exchanges more slowly than the more basic *oxazolone* structure. These trends have also been observed by Wysocki and co-workers in their combined IR-MPD and HDX study on HA $\mathbf{b_2}$ fragments.[71] Clearly, differences in PAs between reagent and analyte ions are not the only parameter affecting HDX rates. Another important parameter is the geometry of the analyte molecule, which enables (or inhibits) the gas-phase HDX mechanism to occur. In the case of low-basicity MeOD, HDX is thought to operate via a "relay" mechanism.[31,89] This mechanism works on the premise that the deuterating molecule simultaneously hydrogen bonds to the proton and a basic site on the peptide. The proton/deuteron transfer then takes place in a concerted mechanism, where the proton is transferred to the deuterating agent, while the deuteron is transferred to the basic hydrogen-bonded site on the peptide. In light of the "relay" mechanism and the results above, it is plausible that a more

(85) Due to spectral congestion, the 1430 cm^{-1} band is rarely a pure CO−H^+ bending mode. Nonetheless, the presence of this moiety is expected to result in strong coupling to other modes and, hence, an increase in the band intensity at this position.

(86) Paizs, B.; Suhai, S. *Mass Spectrom. Rev.* **2005**, *24*, 508–548.
(87) Campbell, S.; Rodgers, M. T.; Marzluff, E. M.; Beauchamp, J. L. *J. Am. Chem. Soc.* **1994**, *116*, 9765–9766.
(88) Gard, E.; Green, M. K.; Bregar, J.; Lebrilla, C. B. *J. Am. Soc. Mass Spectrom.* **1994**, *5*, 623–631.
(89) Wyttenbach, T.; Bowers, M. T. *J. Am. Soc. Mass Spectrom.* **1999**, *10*, 9–14.

flexible *oxazolone* structure more readily assumes the correct geometry for such a concerted mechanism, whereas a *macrocycle* structure is more prone to ring torsion strain, thus raising the transition state energy for this process.

4. Summary and Conclusions

Peptide fragmentation, and sequence "scrambling" in particular, is attracting considerable interest, with for instance a recent focus edition in the *Journal of the American Society for Mass Spectrometry*.[90] Here, the effect of chain length on peptide fragment structure formation is investigated using a range of gas-phase techniques. The data indicate that smaller **b** fragments ($\mathbf{b_2}$, $\mathbf{b_3}$) solely form *oxazolone* structures, whereas midsized fragments ($\mathbf{b_4}-\mathbf{b_7}$) display a mixture of *oxazolone* and *macrocycle* structures. Mixtures of both structures are in fact expected, given that a low-energy isomerization pathway is available to interconvert *oxazolone* and *cyclic* **b** fragment structures.[17,21] This pathway is, however, apparently not available to smaller **b** fragments ($\mathbf{b_2}$, $\mathbf{b_3}$).

In the case of $\mathbf{b_8}$, the IR-MPD and HDX results indicate an exclusive presence of *macrocycle* structures. Moreover, a model *cyclic* hexapeptide, protonated cyclo(Gln-Trp-Phe-Gly-Leu-Met), is also shown to be surprisingly stable and is not subject to isomerization to the *oxazolone* structure. A recent study by Maitre and co-workers had shown that the same $\mathbf{b_5}$ fragment as considered here, but generated from a different precursor ion (G_5R), exclusively gives rise to *macrocycle* structures. This suggests that product ion formation in mass spectrometers is under kinetic control. Moreover, the differences in IR-MPD spectra between $\mathbf{b_5}$-G5 and $\mathbf{b_5}$-G8 presented here emphasize the importance of the precursor ion.

The occurrence of larger *macrocycle* structures in CID is particularly unsettling in terms of sequence "scrambling", since from a statistical point of view larger cyclic structures are more likely to open up at a different site than where they were originally put together. In fact, recent studies by Harrison[91] and Van Stipdonk[43] seem to confirm that larger **b** fragments give rise to considerable sequence scrambling. Sequential fragmentation of larger **b** fragments may hence account for a large fraction of unidentified peaks in tandem mass spectra,[92] and therefore these have to be taken into account to prevent misidentification of proteins.

Complementary information from a range of gas-phase structural techniques was required to establish the qualitative and quantitative trends in the dissociation chemistry presented here. In particular, IR photodissociation spectroscopy allows identification of the chemical species that are generated, whereas H/D exchange enables quantification of the relative amounts that are made. Previous studies had shown that *oxazolone* structures could be readily identified based on the diagnostic *oxazolone* ring C=O stretch.[26,68,69,93] Identification of the *macrocycle* can be established based on the chemically diagnostic $CO-H^+$ bending mode ($\sim$1430 cm^{-1}), even if this mode appears in a potentially more congested region of the IR spectrum. While IR-MPD spectroscopy gives valuable information on the chemical structures of reaction products, such as the chemical moieties formed[26,54,93,94] and the site of proton attachment,[95−97] the IR-MPD yield cannot typically be related to relative abundances of structures in a mixture.

It is demonstrated here that the relative abundances of *oxazolone* and *macrocycle* can be inferred from the kinetic fitting of HDX data. The complementary information from these IR spectroscopy and HDX results allows identification of the *oxazolone* and *macrocycle* $\mathbf{b_5}$-G8 fragment structures present. The results also strongly suggest that *oxazolone* structures display HDX rate constants that are an order of magnitude higher than those of *macrocycle* structures. More heterogeneous cyclic peptide structures, such as protonated cyclo(Gln-Trp-Phe-Gly-Leu-Met), display two distinct "slow" rates, which may be due to different protonation sites or structural variants (e.g., cis/trans). Additional complementary studies by HDX and IR-MPD on different peptide systems will show if a general categorization into "fast" (oxazolone) and "slow" (macrocycle) can be made.

The kinetic fitting HDX method for deducing the relative amounts of chemical structures can potentially play an important role in establishing trends in the chemistry of CID, given its convenient implementation in ion trap mass spectrometers. Ion mobility is another quantitative method for fragment structure analysis that can also play a leading role in this endeavor. Some recent studies, however, have shown that the resolution of ion mobility may not be sufficient to separate and quantify the *macrocycle* and *oxazolone* structures in all cases,[29,30] and possibly HDX can complement those measurements. Additional information from other gas-phase techniques, such as the chemical information from IR spectroscopy, is certainly useful in independently verifying the conclusions from HDX or ion mobility measurements. Ongoing systematic studies will show how prevalent the formation of *macrocycle* fragment structures in CID is. The differences between the present study and the one by Erlekam et al.[27] suggest that the method of ion activation and collisional cooling rates also play an important role in CID chemistry.

Acknowledgment. The authors would like to thank Dr. David Powell for generously providing access to his Fourier transform mass spectrometer (Bruker Daltonics), which was used to carry out the HDX measurements. The skillful assistance of the FELIX staff, in particular Dr. Britta Redlich and Dr. Lex van der Meer, is gratefully acknowledged. Travel support to The Netherlands for N.P. was provided by the NSF-PIRE (NSF-0730072) program to carry out the IR photodissociation experiments with FELIX. The UF HPC Center is acknowledged for providing computational resources and support. N.P. thanks the University of Florida for generous start-up funds. This material is based upon work supported by the National Science Foundation under CHE-0845450. The American Society for Mass Spectrometry (2008 ASMS Research Award) is also acknowledged for their financial support on this project. J.S. and J.O. were supported by the Nederlandse Organisatie voor Wetenschappelijk Onderzoek (Dutch National Science Foundation). Construction and shipping of the FTMS instrument was made possible through funding from the National High Field FT-

(90) Paizs, B.; Van Stipdonk, M. *J. Am. Soc. Mass Spectrom.* **2008**, *19*, 1717–1820.
(91) Harrison, A. *J. Am. Soc. Mass Spectrom.* **2009**, in press.
(92) Simpson, R. J.; Connolly, L. M.; Eddes, J.; Pereira, J. J.; Moritz, R. L.; Reid, G. E. *Electrophoresis* **2000**, *21*, 1707–1732.
(93) Polfer, N. C.; Oomens, J.; Suhai, S.; Paizs, B. *J. Am. Chem. Soc.* **2005**, *127*, 17154–17155.
(94) Frison, G.; van der Rest, G.; Turecek, F.; Besson, T.; Lemaire, J.; Maitre, P.; Chamot-Rooke, J. *J. Am. Chem. Soc.* **2008**, *130*, 14916–14917.
(95) Lucas, B.; Gregoire, G.; Lemaire, J.; Maitre, P.; Ortega, J.-M.; Rupenyan, A.; Reimann, B.; Schermann, J.-P.; Desfrancois, C. *Phys. Chem. Chem. Phys.* **2004**, *6*, 2659–2663.
(96) Lucas, B.; Gregoire, G.; Lemaire, J.; Maitre, P.; Glotin, F.; Schermann, J.-P.; Desfrancois, C. *Int. J. Mass Spectrom.* **2005**, *243*, 97–105.
(97) Simon, A.; MacAleese, L.; Maitre, P.; Lemaire, J.; McMahon, T. B. *J. Am. Chem. Soc.* **2007**, *129*, 2829–2840.

ICR Facility (Grant CHE-9909502) at the National High Magnetic Field Laboratory, Tallahassee, FL, on the initiative of Prof. John R. Eyler and Alan G. Marshall.

Supporting Information Available: Reference 59 is given in full in the Supporting Information. Tables S1 summarizes the electronic and zero-point-corrected energies for the lowest-energy conformers of each chemical structure of $\mathbf{b_2}$. Table S2 summarizes the electronic and zero-point-corrected energies for the lowest-energy conformers of each chemical structure of $\mathbf{b_5}$-G8. Figure S3 shows the vibrational spectra for the 10 lowest-energy conformers for *macrocycle* $\mathbf{b_5}$; the corresponding structures are depicted in Figure S4. The vibrational spectra and corresponding structures for *oxazolone N-prot* are shown in Figures S5 and S6, while the vibrational spectra and structures for *oxazolone ox-prot* are summarized in Figures S7 and S8. The chemical structure of the water loss structure $[M + H - H_2O]^+$, as proposed by O'Hair, is shown in Figure S9. Table S10 summarizes the electronic and zero-point-corrected energies for the lowest-energy protonation site conformers for the water loss structure $[M + H - H_2O]^+$ for $\mathbf{b_5}$-G5. The mid- and near-IR-MPD spectra for $\mathbf{b_5}$-G5 are compared to theoretical spectra for the 5 lowest conformers of $[M + H - H_2O]^+$ *N-term-prot* (Figure S11), $[M + H - H_2O]^+$ *N-ring-prot* (Figure S12), $[M + H - H_2O]^+$ *C═N-prot* (Figure S13), *macrocycle* $\mathbf{b_5}$ (Figure S14), *oxazolone N-prot* (Figure S15), and *oxazolone ox-prot* (Figure S16). Representative H/D exchange mass spectral distributions for $\mathbf{b_2}-\mathbf{b_8}$ are shown in Figure S17. The kinetic fitting results for $\mathbf{b_2}$ to $\mathbf{b_8}$ are summarized in Table S18. Representative H/D exchange mass spectral distributions for $\mathbf{b_5}$-G5 are shown in Figure S19. This material is available free of charge via the Internet at http://pubs.acs.org.

JA9030837